

Electronic structure of a quantum ring in a lateral electric field

J. M. Llorens, C. Trallero-Giner,* A. García-Cristóbal, and A. Cantarero
Material Science Institute, University of Valencia, P.O. Box 2085, E-46071 Valencia, Spain

(Received 30 November 2000; published 20 June 2001)

The electronic states of novel semiconductor quantum rings (QR's) under applied lateral electric fields are theoretically investigated for different values of the ratio r_2/r_1 , where r_2 (r_1) is the outer (inner) radius of the ring. The eigenstates and eigenvalues of the Hamiltonian are obtained from a direct matrix diagonalization scheme. Numerical calculations are performed for a hard-wall confinement potential and the electronic states are obtained as a function of the electric field and the ratio r_2/r_1 . An anomalous behavior in the energy vs. electric-field fan plot due to the break of symmetry is predicted. Analytical expressions for the energy levels, valid in the weak-field limit, are presented and compared with the exact numerical solutions. The effects of decreasing symmetry and mixing on the energy levels and wave functions of the QR due to the applied electric field are also studied. The oscillator strengths of optical transitions between valence and conduction levels are reported as a function of the electric field.

DOI: 10.1103/PhysRevB.64.035309

PACS number(s): 73.21.-b, 71.10.-w, 78.66.Fd, 78.20.Jq

I. INTRODUCTION

Semiconductor zero-dimensional systems obtained by self assembly during epitaxial growth are the subject of extensive experimental studies.¹ The spectroscopic techniques used in these investigations are often combined with the application of external perturbations, such as electric and magnetic fields or hydrostatic pressure,²⁻⁵ which contribute to a better understanding of the observed features because they can remove degeneracies and split or shift the electronic levels. One of the most appealing aspects of the self-assembled nanostructures is given by the enormous possibilities of tailoring their properties by controlling the growth parameters. In view of this, several experimental groups now dedicate their efforts to generate more exotic nanostructures. Thus, for example, vertical ordering in the growth of stacked quantum dot layers has been achieved,^{6,7} which opens the possibility to create quantum dot molecules and superlattices. More recently, the self-assembled growth of flat nanoscopic InAs islands with ringlike shape has been reported.⁸⁻¹⁰ The study of the electronic structure of these novel semiconductor quantum rings (QR's) is particularly interesting due to their nonsimply connected geometry. The preliminary experimental studies on these samples claim for a suitable theoretical modeling of their electronic structure.^{9,10} Though there exists a voluminous body of theoretical work on persistent currents in quantum rings, those studies have been carried out in the mesoscopic regime, where a large number of quantum states is filled.¹¹ Little work has been published so far on the electronic structure of quantum rings in the true quantum limit. The usual approach to date has been to assume a parabolic confinement with an effective radius in the plane of the ring,¹² and several studies of the many-electron problem in a magnetic field have been carried out with this model.¹³ Though giving valuable qualitative results, this approach is far from realistic for the available quantum ring structures, for which the confinement potential is originated from an abrupt material discontinuity.

From the point of view of applications in optoelectronic and tunneling devices, it is essential to investigate the effects

of an electric field on the electronic structure.¹⁴ These sort of studies have been very helpful in the understanding of the electronic properties of bulk and quantum well systems.¹⁵ We believe that experiments performed under the action of electric fields, combined with suitable theoretical modeling, can provide a quantitative way of determining the confinement environment associated with the quantum rings. While the effects of an electric field perpendicular to the ring plane are dominated by the quantum confined Stark effect, as happens in quantum wells,¹⁶ a richer phenomenology is expected when the field is applied in the plane of the ring, since in this case the symmetry of the problem is reduced. In addition, the competence between the field influence and the nontrivial in-plane confinement can lead to new interesting features in the electronic structure. Furthermore, the sensitivity of the electronic structure to a lateral electric field, as opposed to the robustness found for electric fields along the growth direction, can be useful for applications in electro-optical modulation and switching devices. In order to explore these possibilities, we present in this paper a theoretical approach to the electronic states in self-assembled quantum rings under a lateral electric field. A square-shaped confinement potential with infinite barriers is assumed in the calculations.

II. THEORETICAL MODEL

Typical self-assembled ringlike structures present an inner radius r_1 of about 10 nm, while the outer radius r_2 ranges between 30 and 70 nm, and their height L_z is around 2 nm.^{9,10} We consider an electron confined to the circular quantum ring shown in Fig. 1, under the action of an electric field F perpendicular to the Z axis. The characteristic values of the height-to-radius ratio found in the experiments make the toroid of rectangular cross section a good model for the quantum confinement. Within the effective mass approximation, the single-particle Hamiltonian is

$$H = H_0 + e \mathbf{F} \cdot \mathbf{r}, \quad (1)$$

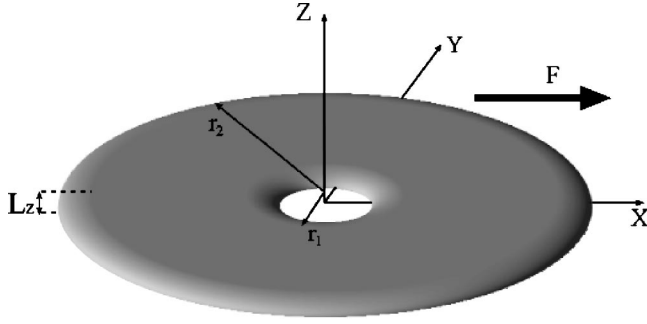


FIG. 1. Schematic picture of a self-assembled quantum ring with dimensions $r_1 = 10$ nm, $r_2 = 50$ nm, and $L_z = 2$ nm. The external electric field F is applied along the X axis.

$$H_0 = p_z \frac{1}{2m_z} p_z + p_\perp \frac{1}{2m_\perp} p_\perp + V(\mathbf{r}, z), \quad (2)$$

where m_z (m_\perp) is the effective mass along the Z axis (in the XY plane), e (>0) is the magnitude of the electron charge, and $V(\mathbf{r}, z)$ is the confinement potential. Here, \mathbf{r} is the radius vector in the XY plane, $\mathbf{r} = (x, y)$. For the case considered here of flat QR's, in which the condition $(r_2 - r_1) \gg L_z$ is fulfilled, we can use the adiabatic approximation where the motion along the Z axis is decoupled from the XY one, disregarding the anisotropic effects due to the corners.^{17,18} Thus, we treat the XY motion as an independent two-dimensional problem and the total wave functions can be factorized as

$$\Psi(\mathbf{r}, z) = \Theta(\mathbf{r}) \Phi_0(z). \quad (3)$$

The function $\Phi_0(z)$ and the energy E_z represent the lower-confined state of the electron by the band profile along the Z axis.¹⁸ As the ring width $r_2 - r_1$ ranges between 20 and 60 nm, an infinite barrier in the ring plane can be safely assumed. Therefore, the eigenfunctions of the in-plane motion for zero electric field can be cast as

$$\Theta_{n,m}^{(0)}(\mathbf{r}) = \frac{e^{im\phi}}{\sqrt{2\pi}} R_{n,m}(r), \quad (4)$$

$$R_{n,m}(r) = A_{n,m} \left[N_{|m|}(\mu_n^{(m)}) J_{|m|} \left(\mu_n^{(m)} \frac{r}{r_1} \right) - J_{|m|}(\mu_n^{(m)}) N_{|m|} \left(\mu_n^{(m)} \frac{r}{r_1} \right) \right]. \quad (5)$$

The normalization constant $A_{n,m}$ is given by

$$A_{n,m} = \sqrt{\frac{2}{\left(\frac{r_2}{r_1}\right)^2 C_m \left(\mu_n^{(m)}, \frac{r_2}{r_1} \right)^2 - C_m \left(\mu_n^{(m)}, 1 \right)^2}}, \quad (6)$$

with

$$C_m(\mu, \alpha) = N_{|m|}(\mu) J_{|m|-1}(\mu\alpha) - J_{|m|}(\mu) N_{|m|-1}(\mu\alpha). \quad (7)$$

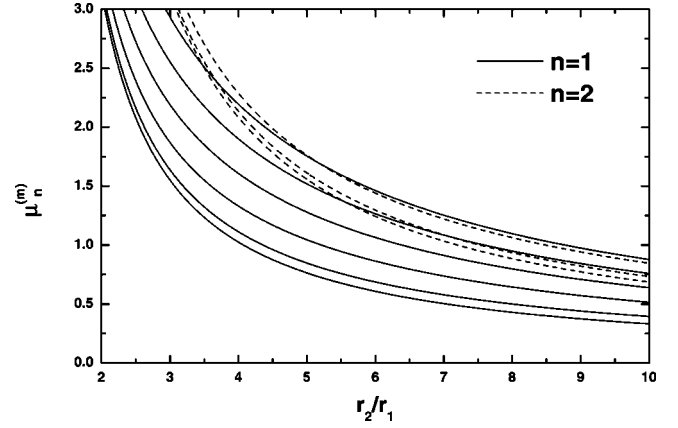


FIG. 2. Eigenvalues $\mu_n^{(m)}$ of Eq. (8) as a function of the ratio r_2/r_1 . Solid and dashed lines correspond to the radial quantum numbers $n=1$ and $n=2$, respectively. The angular momentum m runs from 0 to 5 for $n=1$ and from 0 to 2 for $n=2$. For any value of r_2/r_1 and for a fixed n , $\mu_n^{(m)}$ increases with m .

In these expressions, $J_l(\alpha)$ [$N_l(\alpha)$] is the Bessel (Neumann) function of l th order,¹⁹ $m=0, \pm 1, \dots$, the z component of the angular momentum and $n=1, 2, \dots$, the radial quantum number. The purely two-dimensional (2D) electron energy is $E_{n,m} = E_0 \mu_n^{(m)2}$, where $E_0 = \hbar^2/2m_\perp r_1^2$ and $\mu_n^{(m)}$ are obtained by solving the following secular equation:

$$N_{|m|}(\mu_n^{(m)}) J_{|m|} \left(\mu_n^{(m)} \frac{r_2}{r_1} \right) - J_{|m|}(\mu_n^{(m)}) N_{|m|} \left(\mu_n^{(m)} \frac{r_2}{r_1} \right) = 0. \quad (8)$$

The states (n, m) and $(n, -m)$ are degenerate owing to the cylindrical symmetry of the problem. The eigenvalues $\mu_n^{(m)}$ solution of Eq. (8) are plotted as a function of r_2/r_1 in Fig. 2. They decrease approximately as $(r_2/r_1)^{-1}$ and accidental degeneracies are predicted when two states with different angular momentum m cross for certain values of r_2/r_1 .

The Hamiltonian (1) for a QR under an in-plane electric field $\mathbf{F} = F\mathbf{e}_x$ does not allow for explicit analytical solutions for the wave function $\Theta(\mathbf{r})$. The electric field breaks the axial symmetry and (n, m) are not good quantum numbers anymore. Nevertheless, it is still possible to classify the electron states according to the parity of their wave functions under inversion with respect to the axis of the field (X axis). In other words, there are two disconnected subspaces of *even* [$\Theta(r, -\phi) = \Theta(r, \phi)$] and *odd* [$\Theta(r, -\phi) = -\Theta(r, \phi)$] eigenstates. These subspaces can be obtained separately by expanding $\Theta(\mathbf{r})$ in terms of the corresponding even and odd zero-field eigenstates:

$$\text{even states} \rightarrow \Theta_N(\mathbf{r}) = \sum_{n,m \geq 0} A_{n,m}^{(N)} \frac{\cos(m\phi)}{\sqrt{(1 + \delta_{m,0})\pi}} R_{n,m}(r), \quad (9a)$$

$$\text{odd states} \rightarrow \Theta_N(\mathbf{r}) = \sum_{n,m > 0} B_{n,m}^{(N)} \frac{\sin(m\phi)}{\sqrt{\pi}} R_{n,m}(r), \quad (9b)$$

where N labels the new electronic states in increasing order of the energy E_N , and $A_{n,m}^{(N)}$ and $B_{n,m}^{(N)}$ are coefficients to be determined which ones depend on F and the ratio r_2/r_1 . Substitution of Eq. (9) into Eq. (1) yields two independent systems of dimensionless equations

$$\sum_{n,m \geq 0} \left[\left(\mu_n^{(m)2} - \frac{E_N}{E_0} \right) \delta_{n,n'} \delta_{m,m'} + \frac{1}{2} \frac{F}{F_0} (\delta_{m,m'+1} + \delta_{m,m'-1}) \mathcal{R}_{n',m'}^{n,m} \right] A_{n,m}^{(N)} = 0, \quad (10a)$$

$$\sum_{n,m > 0} \left[\left(\mu_n^{(m)2} - \frac{E_N}{E_0} \right) \delta_{n,n'} \delta_{m,m'} + \frac{\sqrt{(1 + \delta_{m,0})}}{2} \frac{F}{F_0} (\delta_{m,m'+1} + \delta_{m,m'-1}) \mathcal{R}_{n',m'}^{n,m} \right] B_{n,m}^{(N)} = 0, \quad (10b)$$

where $F_0 = E_0 / e r_1$. The matrix elements

$$\mathcal{R}_{n',m'}^{n,m} = \frac{1}{r_1} \int_{r_1}^{r_2} r^2 dr R_{n',m'}(r) R_{n,m}(r), \quad (11)$$

are dimensionless numbers that are evaluated numerically for every value of r_2/r_1 . Equation (10) shows that the electronic states with $\Delta m = \pm 1$ are mixed due to the uniaxial direction introduced by the applied electric field. The eigenstates are obtained by using standard numerical diagonalization techniques to solve Eq. (10).²⁰ In the next section we present numerical results that illustrate the influence of the electric field on the electronic structure of quantum rings of different sizes.

III. NUMERICAL RESULTS

A. Energies and wave functions

In Fig. 3 we plot the calculated energies E_N as a function of the dimensionless electric field F/F_0 for two values of the ratio $r_2/r_1 = 3$ [Fig. 3(a)] and 7 [Fig. 3(b)], representing the smaller and larger rings reported in the experiments.^{9,10} The obtained eigenvalues E_N/E_0 for a given ratio r_2/r_1 are general results that can be particularized to electrons or holes simply by adjusting the value of the effective mass m_\perp . Figures 3(a) and 3(b) show that the effect of the field on the energy increases as r_2/r_1 increases. Otherwise stated, the stronger the confinement, the smaller the electric-field effect. Thus, for the $r_2/r_1 = 3$ case the dispersion of all eigenenergies is very weak, while for the ring with $r_2/r_1 = 7$ the energy dispersion is far more pronounced and exhibits a complex structure with crossings between and anticrossings of the energy levels.

For low electric fields in comparison with the ‘‘unit field’’ F_0 ($F/F_0 \ll 1$), it is possible to obtain approximate analytical expressions for the energies by applying perturbation theory. The energy shifts are found to be quadratic with the field in

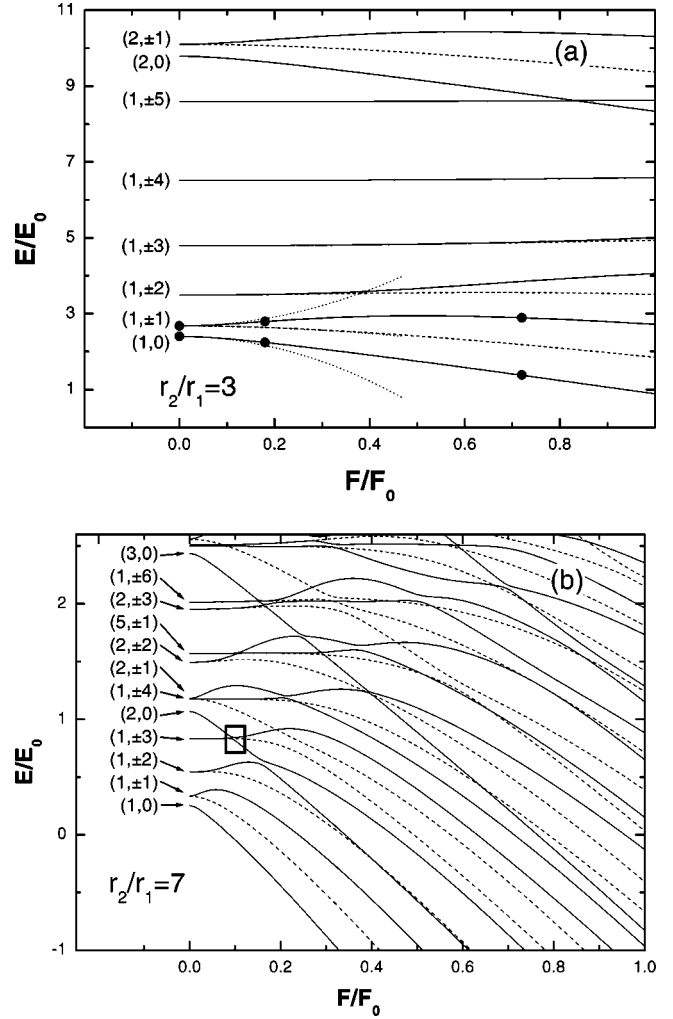


FIG. 3. Energy levels E_N/E_0 of a quantum ring with ratio $r_2/r_1 = 3$ (a) and $r_2/r_1 = 7$ (b), as a function of the dimensionless electric field F/F_0 . The labels on the left of each curve indicate the quantum numbers (n, m) at $F=0$. Solid and dashed lines refer to states with even or odd parity, respectively. The dotted curves in panel (a) represent the approximate results obtained by perturbation theory through Eqs. (12a)–(12c).

the lowest order of approximation. Thus, the energies of the first three levels can be expressed as:

$$E_1(F) = E_{1,0} - 2 \frac{h_{2,1}^2}{E_{1,1} - E_{1,0}} \left(\frac{F}{F_0} \right)^2, \quad (12a)$$

$$E_2(F) = E_{1,1} - \frac{h_{2,1}^2}{E_{1,2} - E_{1,1}} \left(\frac{F}{F_0} \right)^2, \quad (12b)$$

$$E_3(F) = E_{1,1} + \left[2 \frac{h_{1,0}^2}{E_{1,1} - E_{1,0}} - \frac{h_{2,1}^2}{E_{1,2} - E_{1,1}} \right] \left(\frac{F}{F_0} \right)^2, \quad (12c)$$

where $h_{i,j} = \frac{1}{2} \langle R_{1,i} | r | R_{1,j} \rangle E_0$. These energies are also plotted as dotted lines in Fig. 3(a). For very low fields $F/F_0 \lesssim 0.1$ they agree very well with the exact calculations. Nevertheless, for sufficiently high fields the dispersion of the

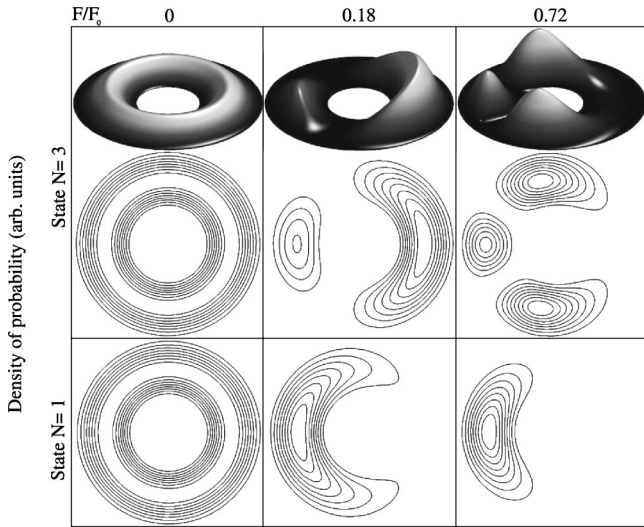


FIG. 4. Contour plots of $|\Theta_N(\mathbf{r})|^2$ ($N=1$ and 3) for a QR with $r_2/r_1=3$, and for three values of the applied electric field, $F/F_0 = 0, 0.18$, and 0.72 . The corresponding 3D plots of $|\Theta_{N=3}(\vec{r})|^2$ are also shown at the top of the figure. The states represented are marked with dots in Fig. 3(a).

energies starts to deviate from the quadratic behavior predicted by Eq. (12), indicating the increasing importance of the nonperturbative field effect. The admixture of states with $\Delta m = \pm 1$ causes a nontrivial behavior in the energy fan plot as a function of F . A given state N can be shifted to lower or higher energy according to the coupling with the $(m \pm 1)$ -th component of the neighboring states with the same parity. In this process the state is forced to reject the $m \pm 1$ level at certain F leading to the reported anomalous oscillations in the energy spectrum seen in Fig. 3(b). The strength of the interlevel coupling is inversely proportional to the energy level separation.

Figure 4 shows the probability density $|\Theta_N(\mathbf{r})|^2$ for the

first two even states ($N=1$ and 3) of a ring with $r_2/r_1=3$, for three different electric fields. The states represented correspond to those marked with dots in Fig. 3(a). At zero electric field, the density of probability presents full axial symmetry. When the field is increased to $F/F_0=0.18$, the function $|\Theta_N(\mathbf{r})|^2$ becomes anisotropic indicating a displacement (polarization) of the electron under the influence of the field: The electron in the ground state $N=1$ moves, as it could be expected, opposite to the direction of the field (that points to the right), but strikingly enough, the electron in the excited state $N=3$ moves in the direction of the field. This fact can be correlated to the energy dispersion shown in Fig. 3(a): The field-induced coupling between the states $N=1$ and $N=3$ shifts up the $N=3$ energy level, while the energy of the $N=1$ state follows a nearly parabolic redshift with the field [see also Eq. (12)]. The upwards dispersion of the $N=3$ state translates into the anomalous polarization of $|\Theta_{N=3}(\mathbf{r})|^2$ reflected in Fig. 4. According to these arguments, one expects that the maximum of $|\Theta_{N=3}(\mathbf{r})|^2$ will cease to move right and start moving left when the field is further increased and the coupling with the next even state $N=5$ forces the energy $E_3(F)$ to recover the downwards dispersion, as shown in Fig. 3(a). This behavior can be indeed recognized in the last panel of Fig. 4, corresponding to $F/F_0=0.72$, where it is apparent that the electron has reversed the direction of its motion.

It is also interesting to explore the evolution of the probability density in the electric-field range around the anticrossing between two energy levels: The region enclosed in the square of Fig. 3(b), in which two electronic states of even parity anticross, is shown in Fig. 5. Incidentally, in this region there is also a state of odd parity whose almost flat dispersion is unaffected by the presence of the neighboring even states, illustrating the independence of both sets of states. The corresponding functions $|\Theta_N(\mathbf{r})|^2$ are also displayed in Fig. 5 for various values of the electric field F/F_0 around the anticrossing between the two even states. At zero

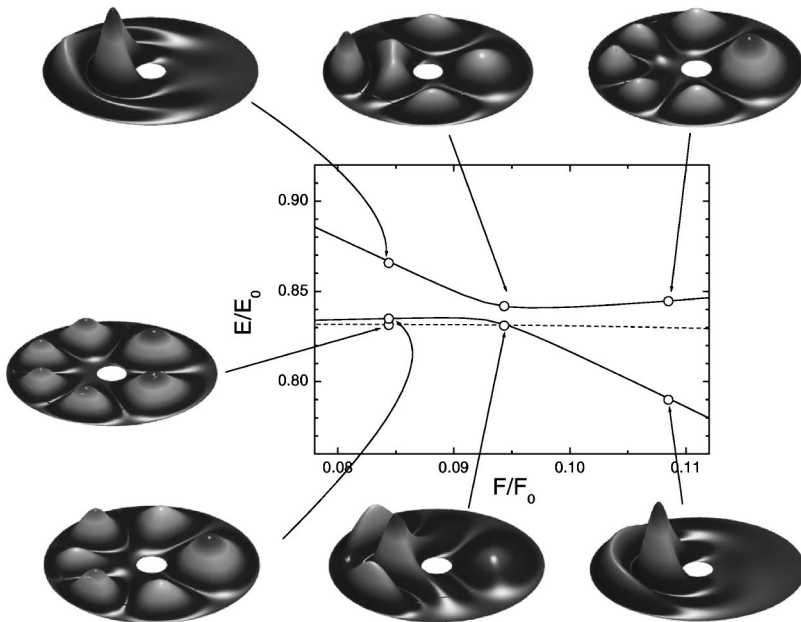


FIG. 5. Enlarged picture of the region enclosed by a square in Fig. 3(b). 3D plots of the probability density for selected states around the anticrossing region are displayed around the graph.

electric field (not shown), the density of probability of all states exhibits full axial symmetry: The two degenerate states are $(n=1, m=\pm 3)$ (with no radial nodes inside the ring) and the other, higher in energy, is $(n=2, m=0)$ (with one radial node). As F/F_0 increases to the value 0.084, the degenerate states of definite (even and odd) parity split in energy. As F/F_0 is further increased, the two even states tend to cross with each other, but this crossing is prevented by their mutual coupling. Instead, there is a strong mixing of both states. This is illustrated in Fig. 5 by the probability densities at $F/F_0=0.094$. Finally, for a value of the field $F/F_0=0.109$, beyond the anticrossing region, it is clearly seen that the functions $|\Theta_N(\mathbf{r})|^2$ of the two even states have completely exchanged their properties.

The electronic states calculated so far apply to experimental situations in which there is only one electron (or hole) per quantum ring. An interesting question concerns the modification of those results when the ring is populated with few electrons. The main effect of the repulsive electron-electron interaction will be a blueshift of the energy levels. This effect will become more pronounced when there is a lateral electric field applied, since then the one-electron wave functions are more localized on one side of the ring (see Fig. 4). One therefore expects that in this case the electronic structure will be determined by the interplay of two opposite effects, i.e., (a) the reported redshift of the one-electron energy levels induced by the electric field (see Fig. 3) and (b) the above-mentioned field-dependent blueshift produced by the electron-electron interaction. In addition, the balance of these two trends will depend on the dimensions of the ring r_1 and r_2 . Detailed calculations are nevertheless needed for a quantitative analysis.

B. Oscillator strengths

An important magnitude for the study of the optical properties is the oscillator strength of the transitions between the valence and conduction states. In our case, it is given by:

$$\int d\mathbf{r} dz \Psi_{N_e}^*(\mathbf{r}, z) \Psi_{N_h}(\mathbf{r}, z) = f_{N_e, N_h} \int dz \Phi_0^{(e)}(z) \Phi_0^{(h)}(z). \quad (13)$$

The in-plane oscillator strength f_{N_e, N_h} is easily evaluated from:

$$f_{N_e, N_h} = \int d\mathbf{r} \Theta_{N_e}^*(\mathbf{r}) \Theta_{N_h}(\mathbf{r}) = \left| \sum_{n,m} A_{n,m}^{(N_e)} A_{n,m}^{(N_h)} \right|^2, \quad (14)$$

where $A_{n,m}^{(N)}$ are the coefficients in the expansion (9). At zero electric field, due to the orthogonality of the wave functions (4), we recover the selection rule $N_e = N_h$ typical of the models with infinite barriers: The oscillator strength matrix is diagonal ($f_{N_e, N_h} = \delta_{N_e, N_h}$) and transitions between electron and hole states with different N are forbidden. When the field is applied, this condition is relaxed and the new symmetry discussed above provides a different selection rule: transitions between even and odd states are forbidden. Since f_{N_e, N_h} involves the field-dependent electron and hole states,

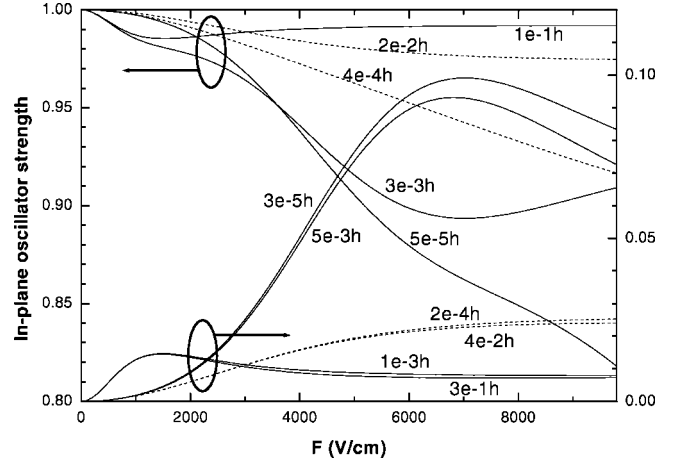


FIG. 6. In-plane oscillator strength for the lowest electron-hole transitions in a quantum ring with $r_2/r_1=3$, as a function of the electric field. The different transitions are labeled by N_e-N_h . Solid and dashed lines correspond to even-even and odd-odd transitions, respectively.

it depends on the electric field, the ratio r_2/r_1 , and the ratio between electron and hole masses. Figure 6 shows the dependence of f_{N_e, N_h} on the electric field for the transitions involving the states $N_e, N_h = 1-5$ in a quantum ring with $r_2/r_1=3$.²¹ The oscillator strengths of even-even and odd-odd transitions are represented with solid and dashed lines, respectively. The transitions 1_e-5_h and 5_e-1_h have negligible oscillator strength and are not displayed. As the electric field increases, the diagonal transitions ($N_e = N_h$) lose oscillator strength, since it is transferred to the nondiagonal ones ($N_e \neq N_h$), which become weakly allowed. This fact is again explained by the field-induced mixing of the various (n, m) components within every state. In general, the field tends to reduce the overlap between electron and hole wave functions. This accounts for the overall reduction of the diagonal oscillator strengths. However, we have seen that the polarization of the wave functions can present anomalies related to the coupling among different states (see Fig. 4). This explains the nonmonotonous field dependence of the oscillator strengths. It should be noticed that the above oscillator strengths correspond to optical transitions neglecting the electron-hole correlation. The inclusion of this interaction will produce a redshift of the transition energies and an increase of the oscillator strengths, which will be a linear combination of f_{N_e, N_h} with different N_e and N_h . Calculations of excitons in quantum rings under an electric field are in progress.

IV. CONCLUSIONS

We have studied theoretically the effects of an electric field applied in the plane of the novel quantum ring structures grown by self-assembly techniques. The electron energies and wave functions have been calculated within the envelope-function approximation. The results are expressed very generally in terms of only two dimensionless parameters, the ratio r_2/r_1 and the normalized field F/F_0 , and

represent a first step for further investigations of several physical magnitudes. We find that due to the break of axial symmetry by the field, the energy levels of large quantum rings exhibit a complex dispersion as a function of the electric field. We have also studied the field-induced polarization of the electron wave functions and found an anomalous behavior that can be correlated with the energy dispersion. We have also calculated and analyzed the field dependence of the oscillator strength for a number of optical transitions between valence and conduction states. The geometry-

dependent features identified in our calculations can be used to estimate the size of the available quantum rings structures.

ACKNOWLEDGMENTS

One of us (C.T.-G.) acknowledges the financial support of the University of Valencia. The work has been partially financed by Grant No. GV00-080-15 of the Generalitat Valenciana and Grant No. MAT2000-0772-C02-01 of the Ministerio de Ciencia y Tecnología (Spain).

*Permanent address: Department of Theoretical Physics, Havana University, Vedado, 10400, Havana, Cuba.

¹D. Bimberg, M. Grundmann, and N. N. Ledentsov, *Quantum Dot Hetrostructures* (Wiley, Chichester, 1998).

²A. Babinski, A. Wyszomolka, T. Tomaszewicz, J. M. Baranowski, R. León, C. Lobo, and C. Jagadish, *Appl. Phys. Lett.* **73**, 2811 (1998); I. E. Itskevich, S. I. Rybchenko, I. I. Tartakovskii, S. T. Stoddart, A. Levin, P. C. Main, L. Eaves, M. Henini, and S. Parnell, *ibid.* **76**, 3932 (2000).

³M. Sugisaki, H. W. Ren, K. Nishi, S. Sugou, T. Okuno, and Y. Masumoto, *Physica B* **258**, 169 (1998); A. García-Cristóbal, V. M. Fomin, and J. T. Devreese, *ibid.* **258**, 190 (1998); M. Bayer, O. Stern, A. Kuther, and A. Forchel, *Phys. Rev. B* **61**, 7273 (2000).

⁴J. Phillips, A. Bhattacharya, and U. Venkateswaran, *Appl. Phys. Lett.* **74**, 1549 (1999).

⁵M. S. Skolnick, I. E. Itskevich, P. W. Fry, D. J. Mowbray, L. R. Wilson, J. A. Barker, E. P. O'Reilly, I. A. Trojan, S. G. Lyapin, M. Hopkinson, M. Al-Khafaji, A. G. Cullis, G. Hill, and J. C. Clark, *Physica E (Amsterdam)* **6**, 348 (2000).

⁶Q. Xie, A. Madhukar, P. Chen, and N. Kobayashi, *Phys. Rev. Lett.* **75**, 2542 (1995); N. N. Ledentsov, V. A. Shchukin, M. Grundmann, N. Kirstaedter, J. Bohrer, O. Schmidt, D. Bimberg, V. M. Ustinov, A. Y. Egorov, A. E. Zhukov, P. S. Kopev, S. V. Zaitsev, N. Y. Gordeev, Z. I. Alferov, A. I. Borovkov, A. O. Kosogov, S. S. Ruvimov, P. Werner, U. Gosele, and J. Heydenreich, *Phys. Rev. B* **54**, 8743 (1996).

⁷R. Heitz, A. Kalburge, Q. Xie, M. Grundmann, P. Chen, A. Hoffman, A. Madhukar, and D. Bimberg, *Phys. Rev. B* **57**, 9050 (1998); R. Heitz, I. Mukhametzhano, J. Zeng, P. Chen, A. Madhukar, and D. Bimberg, *Superlattices Microstruct.* **25**, 97 (1999).

⁸J. M. García, G. Medeiros-Ribeiro, K. Schmidt, T. Ngo, J. L. Feng, A. Lorke, J. Kotthaus, and P. M. Petroff, *Appl. Phys. Lett.* **71**, 2014 (1997).

⁹A. Lorke and R. J. Luyken, *Physica B* **256-258**, 424 (1998); A. Lorke, R. J. Luyken, M. Fricke, J. P. Kotthaus, G. Medeiros-

Ribeiro, J. M. García, and P. M. Petroff, *Microelectron. Eng.* **47**, 95 (1999); H. Pettersson, R. J. Warburton, A. Lorke, K. Karrai, J. P. Kotthaus, J. M. García, and P. M. Petroff, *Physica E (Amsterdam)* **6**, 510 (2000).

¹⁰A. Lorke, R. J. Luyken, A. O. Govorov, J. P. Kotthaus, J. M. García, and P. M. Petroff, *Phys. Rev. Lett.* **84**, 2223 (2000); R. J. Warburton, C. Schaflein, D. Haft, F. Bickel, A. Lorke, K. Karrai, J. M. García, W. Schoenfeld, and P. M. Petroff, *Nature (London)* **405**, 926 (2000).

¹¹U. Eckern and P. Schwab, *Adv. Phys.* **44**, 404 (1995).

¹²T. Chakraborty and P. Pietiäinen, *Phys. Rev. B* **50**, 8460 (1994); V. Halonen, P. Pietiäinen, and T. Chakraborty, *Europhys. Lett.* **33**, 377 (1996).

¹³A. Emperador, M. Barranco, E. Lipparini, M. Pi, and L. Serra, *Phys. Rev. B* **59**, 15 301 (1999); A. Emperador A, M. Pi, M. Barranco, and A. Lorke, *ibid.* **62**, 4573 (2000).

¹⁴A. M. Fox, *Contemp. Phys.* **37**, 111 (1996); J. E. Cunningham, *Mater. Sci. Eng. R.* **25**, 155 (1999).

¹⁵F. H. Pollak and H. Shen, *Mater. Sci. Eng. R.* **10**, 275 (1993); H. Shen and M. Dutta, *J. Appl. Phys.* **78**, 2151 (1995).

¹⁶D. A. B. Miller, D. S. Chemla, T. C. Damen, A. C. Gossard, W. Wiegmann, T. H. Wood, and C. A. Burrus, *Phys. Rev. B* **32**, 1043 (1985).

¹⁷F. M. Peeters and V. A. Schweigert, *Phys. Rev. B* **53**, 1468 (1996).

¹⁸E. Menéndez-Proupin, C. Trallero-Giner, and S. E. Ulloa, *Phys. Rev. B* **60**, 16 747 (1999).

¹⁹P. M. Morse and H. Feschbach, *Methods of Theoretical Physics* (McGraw-Hill, New York, 1953).

²⁰E. Casado and C. Trallero-Giner, *Phys. Status Solidi B* **196**, 335 (1996).

²¹In the calculations of the oscillator strengths we have employed the InAs effective masses reported in *Landolt-Börnstein Numerical Data and Functional Relationships in Science and Technology* (Springer, New York, 1982): $m_e = 0.023m_0$ and $m_{hh,1} = 0.036m_0$ (m_0 is the free-electron mass).